Integrative and Comparative Biology

*Integrative and Comparative Biology*, volume 52, number 5, pp. 597–615
doi:10.1093/icb/ics113

*Society for Integrative and Comparative Biology*

SYMPOSIUM

# Swimming in the Intermediate Reynolds Range: Kinematics of the Pteropod *Limacina helicina*

Yin Chang* and Jeannette Yen[1,†]

*BC Centre for Disease Control, Vancouver, BC, Canada; †School of Biology, Georgia Institute of Technology, Atlanta, GA 30332, USA

From the symposium "Combining Experiments with Modeling and Computational Methods to Study Animal Locomotion" presented at the annual meeting of the Society for Integrative and Comparative Biology, January 3–7, 2012 at Charleston, South Carolina.

[1]E-mail: jeannette.yen@biology.gatech.edu

**Synopsis** *Limacina helicina* (1–3 mm) lives in the environment that straddles both inertial and viscous regimes. In this intermediate Reynolds range ($10^0$–$10^3$), an oscillating appendage may use either drag-based or lift-based locomotion. The swimming motion of *L. helicina* was investigated to determine its mechanics and whether features of rowing or flying gaits were present. Mean speeds, stroke frequencies, and general paths were revealed from the trajectories of free-swimming individuals. High-speed videography of tethered animals enabled a detailed analysis of stroke parameters involved in *L. helicina* swimming. During swimming episodes, *L. helicina* ascend along a sawtooth trajectory in mostly linear and sometimes helical paths. Mean speeds varied from 13 to 44 mm/s for straight ascents and slightly more for helical paths. During swimming, the stroke cycle caused oscillations in body orientation, whereas sinking is characterized by smooth straight descents. Sinking speeds of 5–45 mm $s^{-1}$ were observed. Wing-beat frequencies decreased with body size from 4.5 to 9.4 Hz. The wing stroke is a complex, three-dimensional motion that does not perfectly correspond to theoretical concepts of drag-based or lift-based propulsion. Instead, the repertoire of movements indicates that elements of both rowing and flying are incorporated in the swimming of *L. helicina* with the added element of rotation. Size-dependent differences in stroke mechanics are described. Of particular note is evidence that a clap-and-fling mechanism is applied during the stroke cycle.

## Introduction

Organisms that live in the intermediate Reynolds ($Re = 10^0$–$10^3$) range are affected by both inertial and viscous forces. Depending on the Re at which an animal functions, oscillating appendages may use drag-based or lift-based locomotion. With decreasing body size, increasing viscous forces could attenuate the degree of circulation needed to generate lift (Walker 2002). The ratio of lift to drag decreases with small Re; thus, the thrust that can be produced also diminishes. These effects have prompted the scaling hypothesis that small, slow animals should row their appendages to take advantage of the dominance of viscosity to produce thrust (Horridge 1956; Walker and Westneat 2000; Walker 2002).

Rowing is an energetically cheap mechanism that incorporates passive mechanisms, such as changes in the paddle's surface area and reduction in limb span to generate thrust (Walker 2002). In the power stroke, the rowing limb increases its drag by either maximizing its surface area or by orienting into a high-drag position. The resultant net thrust is generated as the limb minimizes its surface area or orients into a position of least drag in the recovery stroke. The feathering of webbed fins is used by fish and freshwater turtles to create this differential thrust in the stroke cycle. Hairy appendages also function as excellent paddles to create this asymmetry of stroke and are used by zooplankton such as *Daphnia* sp., copepods, and euphausiids. A triangular-shaped paddle with the distal margin forming the blunt edge is modeled as the shape with the maximum efficiency for drag-based propulsion (Blake 1981).

Advanced Access publication September 16, 2012

In contrast, lift-based propulsion is associated with a wing-like limb that tapers at its distal end (Combes and Daniel 2001). In this locomotor mode a lift force, comprising both a thrust and weight support, is directed perpendicular to the direction of movement; thrust can either be generated in the downstroke or continuously throughout the stroke. Flapping cannot make use of viscous forces, requiring the large bound and vortex forces available at high Re (Dickinson 1996). Therefore, flapping is normally a gait utilized by large marine animals and has been noted in the movements of rays and fishes (Webb 1973; Daniel 1988; Gibb et al. 1994; Drucker and Jensen 1996; Rosenberger and Westneat 1999) as well as of aquatic birds, turtles, and mammals (Clark and Bemis 1979; Renous and Bels 1993; Fish 1996; Johansson and Aldrin 2002). Less explored is the notion of flight in aquatic invertebrates—with the only studied example being *Clione*, a neutrally-buoyant shell-less gymnosome pteropod (Satterlie et al. 1985; Childress and Dudley 2004; Borrell et al. 2005; Szymik and Satterlie 2011).

Here we present a study of the shelled thecosome *Limacina helicina*, a species of pteropod that lives exclusively in the plankton, is small, swims slowly, and is an excellent study animal for assessing locomotion in the intermediate Re range. Swimming occurs with the ventral surface up and the footlobes and wings extended from the shell's aperture (Lalli and Gilmer 1989). Morton (1954) described the motion of a related species, *Limacina retroversa*, as swimming with a vertically-oriented rowing gait with repeated upward motions that follow a spiral course. It thus seems conceivable that *L. helicina*, although dissimilar in shell structure, also uses a rowing gait. The calcareous shell of *L. helicina* adds enough negative buoyancy that active flapping of the wings is necessary to keep the animal from sinking. Walker (2002) suggested that lift-based flapping may be the preferred locomotor mode, despite increased costs and decreased efficiency at low Re. Strategies that overcome the large viscous forces of low Re were previously suggested for the flight of other diminutive fliers (e.g., Weis-Fogh 1973; Ellington 1984; Dickinson et al. 1999; Miller and Peskin 2004). Swimming, showing elements of both drag-based and lift-based mechanisms, is alternated with slow sinking during which the wings do not flap. *In situ* observations have found motionless animals supported by large, spherical mucus feeding webs (Gilmer and Harbison 1986), produced by the pteropod to capture fine particles. Large movements would be disruptive to such feeding structures. The lack of motion indicates that this mucus parachute perfectly offsets the weight of the pteropod and its shell.

*Limacina helicina* appears able to sense turbulent motion, where disturbances created by the slight movements of nearby scuba divers, or a predatory fish, elicit escape reactions with speeds up to 12 cm/s for Arctic individuals (Gilmer and Harbison 1986), leaving the mucus web behind. For *L. helicina*, swimming is essential for both escape behavior and diel migrations that often encompass hundreds of meters a day for limacinids (Wormuth 1981; Comeau et al. 2010). Since the wing of *L. helicina* is not bristled like those of most rowing appendages, characteristic rowing mechanics would be unexpected. Novel unsteady mechanisms that augment lift may support the swimming of this negatively buoyant animal. The purpose of this work is to determine the characteristics of the wing stroke and describe the kinematic properties of the unusual locomotory tactics of *L. helicina*.

## Materials and methods

### Collection of specimens

*Limacina helicina* was collected and filmed aboard ship during a cruise on the R/V Point Sur in the Santa Barbara Channel between July 29 and August 8, 2002. Oblique tows at night were made from depths of 80 m using a 1-m-diameter 500-μm mesh plankton net. *Limacina helicina* appeared as darkly-pigmented particles in the bottom of the tow and were easily sorted from the remainder of the plankton. Individuals were separated by size and used immediately for shipboard filming. The patchiness and fragility of this species precluded measurements to be repeated after this cruise, despite many attempts to collect and ship these organisms to our laboratory.

### Filming

The three-dimensional swimming behavior of 20–30 freely swimming pteropods was quantified from videosequences recorded on two Pulnix analog videocameras (30 frames per second) fitted with 60-mm lenses and positioned to obtain orthogonal views of a 0.32 L volume situated within a 1.0 L total volume at least 14 mm from any surface to avoid wall effects in a 78 mm × 78 mm × 285 mm (length × width × height) tank filled to a height of about 170 mm with channel seawater at ambient temperatures of 14.5–16.0°C. High magnification views of the parapodial movements of three pteropods, individually tethered to a 147-μm wire (Fig. 1),

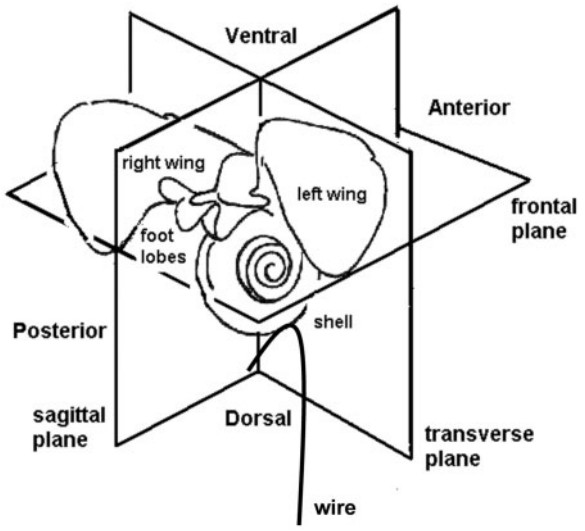


**Fig. 1** Anatomical features and planes of *L. helicina*.

were recorded on a high-speed digital video camera (Redlake at 250 fps). Infrared diodes (LED, 880 nm) supplied the illumination for each of 4-h-long video sequences. After filming concluded, the animals were preserved in 70% ethanol or frozen and dried at 60°C.

### Video and data analysis

Three-dimensional positions every 0.033 s from digitized videosequences provided ($x$,$y$,$z$,$t$) data to calculate the swimming velocity of pteropods along straight or helical paths ($U_{swim}$, $U_{helix}$) (Stokes 1997), their sinking speeds ($U_{sink}$), and wingbeat frequency. Wingbeat frequencies were visually-determined as the inverse of the period for a complete wing stroke cycle, averaged from three to eight cycles for 13 sequences for each individual. The $z$-axis was the vertical axis for the animal and was the usual forward direction of movement (Fig. 2). In other words, *L. helicina* typically travels upward but was tethered so that this upward movement was evaluated as forward horizontal motion.

Locomotory kinematics of tethered animals were based on measurements every 0.008 s of their wingtip coordinates, angular displacement of the wingtip ($\alpha$) and wing chord ($\beta$), angular velocity ($\omega$), and wingbeat frequency ($\eta$). To correct for the movements of the body that occurred with each wing stroke, additional body landmarks were used to determine wing displacement (Fig. 2A). To examine chordwise changes in wing amplitude, a stroke angle was calculated for both the wingtip ($\theta$) and midline wing chord ($\beta$). The wingtip marker was the distal portion of the wingtip while the wing chord marker was the portion of the (midline) wing chord; the latter marker was evident in the large specimen as a visible notch midway along the wing's surface. Angles were in reference to an anterior shell marker ($E$) and the position of the wing at the onset of the recovery stroke, such that angles increased during the recovery stroke with a positive velocity and decreased during the power stroke with a negative velocity (Fig. 2B). Angular velocity was calculated as the change in angular displacement during 0.008 s. Wingbeat frequencies were verified with the angular displacement data.

Morphological measurements of diameter, wingspan, length of the wing chord, and wing area were taken from footage of the tethered animals, not from microscopic analyses as wing tissue did not preserve well. Movies in Supplementary Data show differences noted in wing kinematics, shapes, and swimming trajectories of the large, medium, and small pteropods. The diameter of the shell (l) was determined by measuring the distance along the anterior–posterior axis to the outer whorl. Wingspan ($b$) was the distance from tip to tip of outstretched wings. Since the chord length of *L. helicina* varies from root to tip of the wing, two chord lengths were taken: the midline wing chord ($d_m$) and the wingtip chord ($d_t$). The aspect ratio (AR), calculated as $[b/d]$ where $b$ = wing span (mm) and d = chord length (mm), was used to compare wing shapes for different sized individuals.

The advance ratio ($J$), used to relate the forward speed to the rotational speed of the wing, was computed as

$$J = \frac{U_{swim}}{2\,\alpha\eta d}$$

where $U_{swim}$ = forward swim speed (mm/s), $\alpha$ = stroke angle (rad), $\eta$ = stroke frequency (Hz), and $d$ = tip chord length (mm).

The regression equation of size with mean swimming speed provided the mean forward swimming speeds that tethered animals could theoretically achieve. This value was used to determine the advance ratio for that individual.

The Re of free-swimming animals ($Re_b$) was compared to that of the wing motion of the tethered animals ($Re_w$) and was computed as $Re = (U\ \ell)\nu^{-1}$. The parameter U was either the forward swim speed or wing speed (mm/s), $\ell$ = shell length or wing length (mm), and $\nu$ = kinematic viscosity (at 16°, $\nu = 1.17 \times 10^{-6}\ m^2/s$).

Statistical analyses (SigmaPlot 7.0) included a least squares regression applied to the variables of mean swimming speed, mean sinking speed, Reynolds number and wingbeat frequency against the length of shell to identify trends between parameters, a

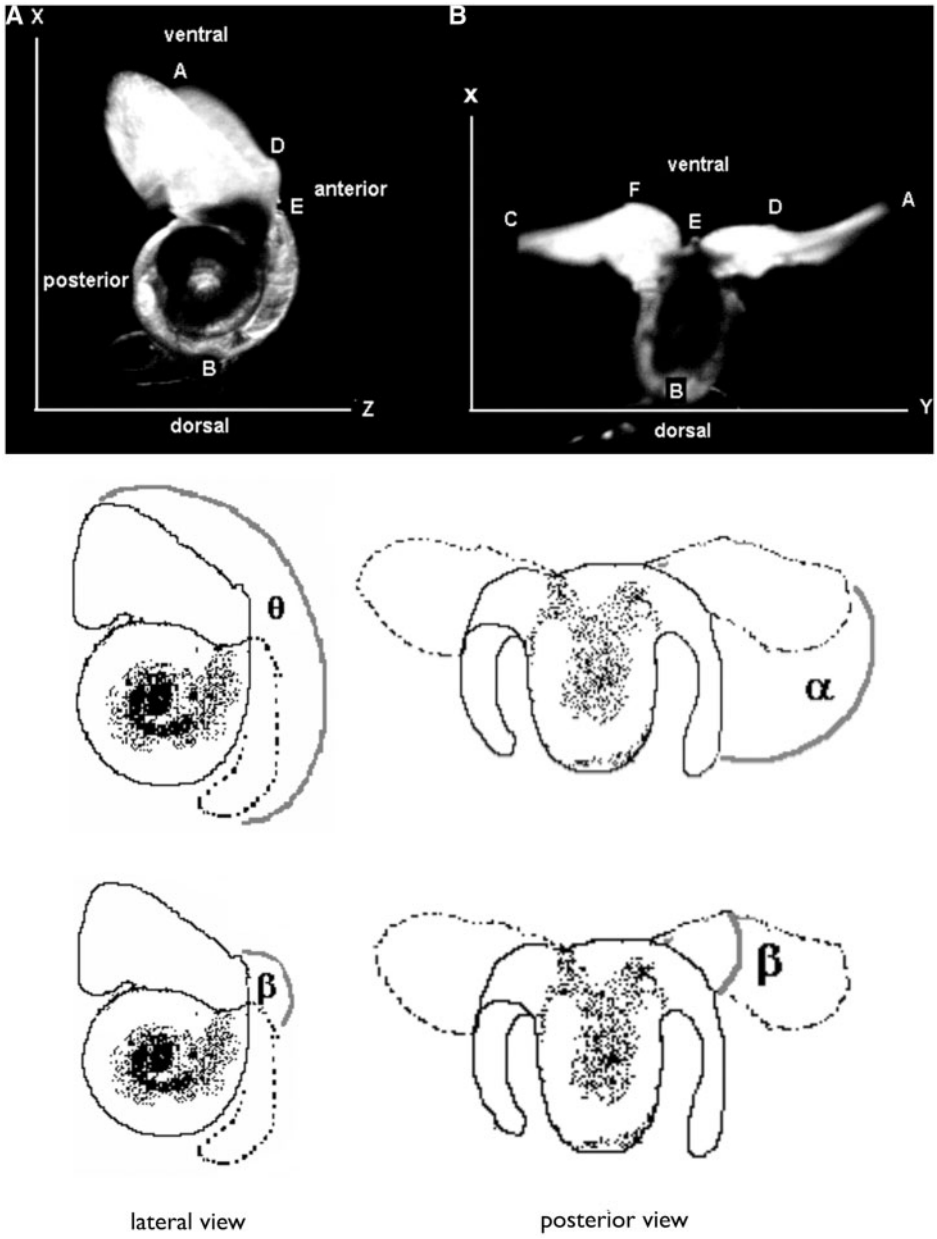


**Fig. 2 Upper:** Positional markers used for kinematic analysis of *L. helicina* from lateral (A) and posterior (B) views. Reference points used for kinematic tracking included: A, the marker for the tip of the left wing; B, the bottom body position; C, the right wingtip; D, the left wing chord; E, the marker for the ventral body position, and; F, the right wing chord. **Lower:** Illustration of angle measurements taken for the pteropod kinematic analyses.

Wilcoxon paired-sample test to test for differences between the power strokes and recovery strokes of the tethered animals, and a one-way analysis of variance to test for significant differences in kinematic quantities among these tethered individuals. Student's *t*-tests were applied to test for dissimilarity between the kinematics of the left and right wings, between the kinematics of the power strokes and recovery strokes, and between the angular velocities of animals from similar views. All values are reported as mean ± 1 SD.

## Results

### Morphology of *Limacina helicina*

The wings of *L. helicina* are flat, continuous membranes that project posterior-laterally from either side of the shell and dynamically change shape during the wing stroke. The wing chord varies along the length of the wing with a large distal area, followed by a smaller medial section, and a connection to the rest of the body that is slender. Using the wingtip chord, there is little difference in

**Table 1** ARs and wing loadings for the three tethered *L. helicina* used in this study

| Shell diameter(mm) | AR** (mid chord) | AR (chord tip) |
|---|---|---|
| 3.10 | 5.78 ± 0.53 | 3.79 ± 0.34 |
| 1.98 | 7.28 ± 0.87 | 3.03 ± 0.36 |
| 0.94 | 8.66 ± 0.62 | 3.20 ± 0.23 |

Means and standard deviations are from five measurements taken from the films of the three pteropods.
**$P < 0.001$; analysis of variance of the AR between the three animals.

AR between the three tethered animals utilized in this study (Table 1). On the other hand, using the medial wing chord, the differences are much more defined and there is an inverse relationship between size and AR, indicating that small individuals have longer, thinner wings while the wings of larger specimens are shorter and stouter. Indeed, the wings of the small individual seem more stalked with a narrow base while the larger wings are generally more triangular.

### Kinematics of swimming in freely swimming *Limacina helicina*

Swimming in *L. helicina* (1.24–3.38 mm) consists of surprisingly straight upward trajectories in addition to curved and spiral paths. Brief periods of hovering, inevitably disrupted by movement in some direction, were observed in video sequences. Ascents are made with continuous flapping of the wings followed by rapid sinking with immobile wings trailing behind, offering little resistance to downward movement. To arrest the descent, the animals simply extend their wings laterally and are able to resume upward movements almost immediately.

The majority of the analyzed paths were characteristically straight with swimming speeds varying from a low of 13 mm/s to a maximum of 44 mm/s for a 2.8-mm specimen ($r^2 = 0.57$, $P = 0.0001$; Fig. 3B). Speeds while sinking were from 5 mm/s to a peak of 45 mm/s and remained high for the most part for larger sized pteropods ($r^2 = 0.52$, $P < 0.0001$; Fig. 3C). Swimming speeds slightly exceeded sinking speeds for small individuals but were quickly surpassed by sinking rates in animals larger than 2.0 mm, when sinking was faster. For the few animals that displayed helical paths that remained within view of both cameras, their speeds increased with size in a nonlinear fashion, rising exponentially with increase in shell size ($r^2 = 0.89$, $P < 0.001$; Fig. 3A). Speeds of animals with helical trajectories fell below those of individuals that travelled straight or curved paths for *L. helicina* of the same size up to 2.2 mm but surpassed these speeds (up to ~55 mm/s) in larger animals (Fig. 3A and B). Reynolds numbers calculated from these velocities steadily increase with large body size and range from 20 to 110 ($r^2 = 0.86$, $P < 0.0001$; Fig. 4).

Wingbeat frequencies of 4.5–9.4 Hz had an inverse relationship with size ($r^2 = 0.71$, $P < 0.0001$; Fig. 5) for both free-swimming and tethered animals. Errors for the smaller specimens are large due to the inherent difficulty in seeing small wings as well as the lower resolution of the videos of freely swimming pteropods.

### Wing stroke cycle of freely swimming and tethered *Limacina helicina*

For the freely swimming pteropod, the ascent takes an uneven trajectory as a result of the rotational effects of the stroke cycle on body orientation of *L. helicina*. During the recovery stroke, the wings move synchronously upward on either side of the shell. In the downward motion of the power stroke, the wings return to their positions alongside the shell (Figs. 6–10). When viewed from the morphological left side during intervals of unrestrained swimming, the recovery stroke causes a counterclockwise rotation of the body until the wings reach their maximum stroke amplitude at the beginning of the power stroke. The downward movement of the wings then reverses the rotation so that the body turns clockwise until the wings are midway into the power stroke. Throughout both the recovery stroke and part-way through the power stroke, the body moves upward at an oblique angle, where the rotational movement produces thrust on both strokes and some propulsive force is lost in the spinning motion. Vertical thrust is generated when the wings orient perpendicularly to the mean direction of motion halfway through the power stroke; the wings then adduct to finish the power stroke. In this way, wing rotations do not cancel each other and the animal is able to move upward, albeit in a slightly oblique manner. Thus, it appears that the animal propels its way forward (or upward) using a combination of negative and positive pitching that is activated by the movements of the wings. These rotations were evident in the video of certain large, freely swimming specimens. However, it is unclear if these movements are consistent for all sizes of *L. helicina* as the fine rotational movements of the smaller animals were difficult to observe at the magnification used.

To get a closer look at the wing movements of *L. helicina*, three specimens, hereafter referred to as the large, medium, and small pteropods (3.10, 1.98

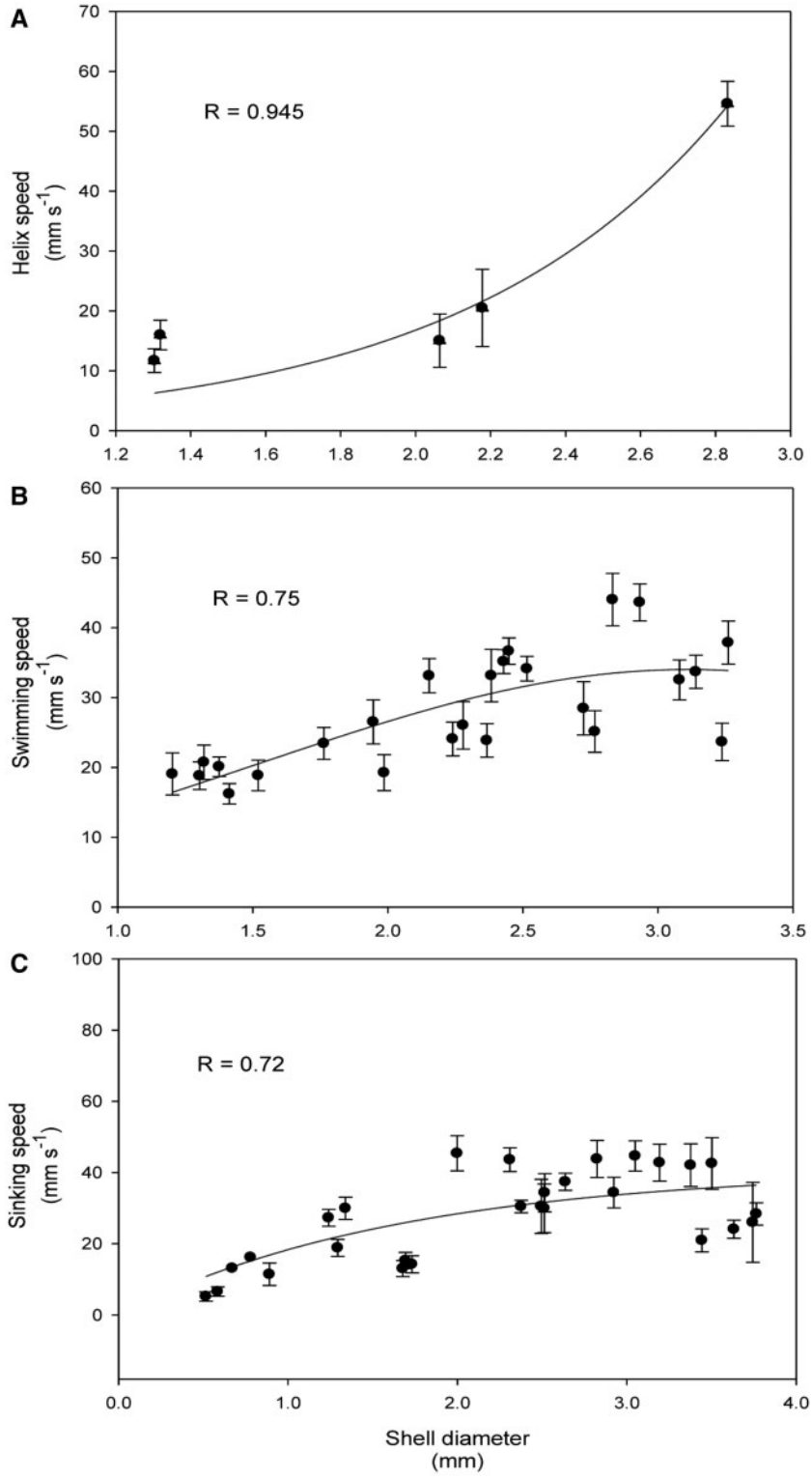


**Fig. 3** Kinematics of free-swimming *L. helicina*. Swimming speeds of individuals that swam in a spiral manner, $U_{helix}$ (A) and a nonspiral manner, $U_{swim}$ (B). Sinking speeds of *L. helicina* also are presented, $U_{sink}$ (C). Each of the 30 points represents the mean speed of a single individual of that size based on 20–100 velocity measurements along its trajectory.

and 0.94 mm in shell size respectively), were filmed with a high-speed camera. Since these images could not be combined with those of the lower resolution camera, only two-dimensional information was available. From these videos, suitable image sequences were made from different perspectives of the three animals: large (posterior, lateral); medium (ventral); and small (lateral). The tether limited the full body

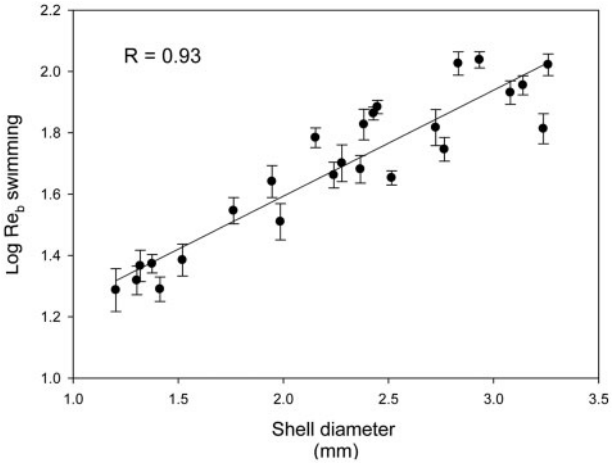


**Fig. 4** Reynolds numbers ($Re_b$) for swimming speeds of *L. helicina* illustrated in Fig. 3B.

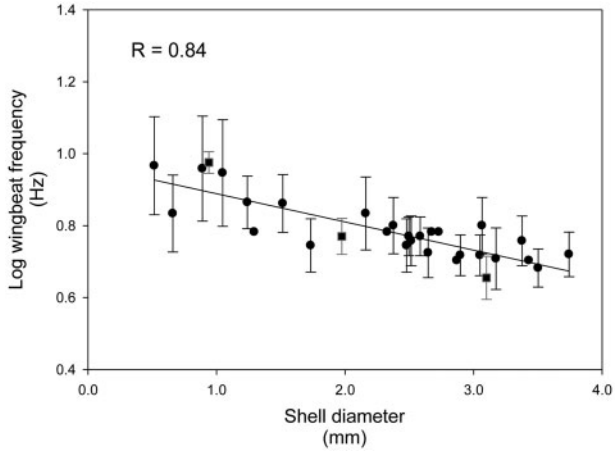


**Fig. 5** Wingbeat frequencies ($\eta$) of free-swimming (filled circle) and tethered (filled square) *L. helicina*. Means and standard deviations are from 8 to 14 cycles/individual. When frequencies are regressed against $\log_{10}$ shell diameter, the relationship has a slope of −0.31.

rotation that occurs throughout the stroke cycle. Figures 6–10 illustrate the wing motion of *L. helicina* relative to its body.

The wing action of the three tethered pteropods was distinct. For the large *L. helicina*, wings move along the transverse plane at the onset of the recovery stroke where they are flattened in full extension (Figs. 6b–c and 7 b–c). A switch directly into the sagittal plane follows where wings make contact at the end of the recovery stroke (Figs. 6d–f and 7 d–f). The trajectory of the wingtips in the power stroke lies above that of the previous path of the wing as the wings separate and move through the sagittal plane once again (Fig. 8A). Midway through the power stroke, however, the wings pronate so that they are perpendicular to the dorsoventral axis of the body, adducting to finish the power stroke along a path that is more proximal to the body than that during the recovery stroke (Figs. 6i, 7k and 8 A). Likewise, the medium-sized individual also performs a wing twist midway into its power stroke (Fig. 9h–i), but does not appear to rotate its wings at the beginning of the recovery stroke. In dorsal view, the path of the wing of the medium-sized animal resembles that of the large animal although there is less deviation between power and recovery stroke paths (Fig. 8B). In contrast, for the small animal there is neither wing rotation nor spanwise twisting of the wing during its wing stroke, which follows the same path about the dorsoventral axis quite faithfully both during the power stroke and the recovery stroke (Figs. 8D and 10). Comparatively, the lateral view of the large animal's wingtip path clearly shows how separate the two half strokes are and further demonstrates that there are changes in the geometry of the stroke (Fig. 8C). There is greater restriction of the wing to one plane in the small animal, suggesting that thrust also is maintained in one direction. Furthermore, the small wing is oriented nearly perpendicular to the dorsoventral axis of the body during the power stroke, thereby maximizing thrust that can be generated (Fig. 10h). The larger individual, although also appearing to orient its wings in an orthogonal manner in the middle of its power stroke (Fig. 6i), has a large flexible surface area at the distal portion of its wing. The smaller AR (when the tip is used) of the large wing is in contrast with that of the small pteropod, implying that there may be a decreased efficiency in this thrust-producing surface as much momentum may be lost along the tips.

The timing of the recovery and power strokes is significantly different for all three *L. helicina* observed (Table 2). The power stroke for the large and small animals takes longer compared to their recovery periods, and the medium-sized animal has the reverse trend. However, when total period is compared, the large and medium-sized pteropods do not vary from one another; the period of the small individual does differ significantly from that of the other two.

The tethered pteropods appear to utilize a clap-and-fling mechanism, in which the wings clap together at the end of the upstroke and then are peeled apart at the initiation of the downstroke. At the end of the recovery stroke, the wings come together and make contact posteriorly in the sagittal plane, during the ventral ''clap'' phase (Figs. 6f, 7f, 9f

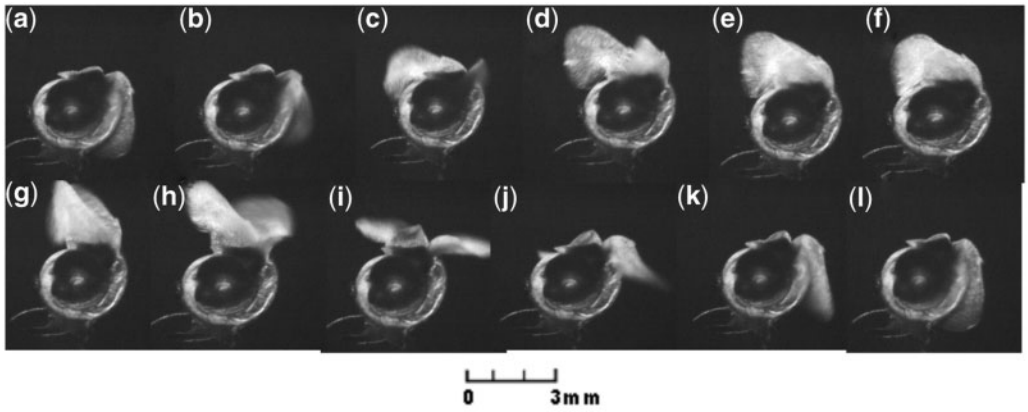


**Fig. 6** Lateral view of the stroke cycle of a large, tethered *L. helicina* starting from the recovery stroke. There are 16 ms between each frame shown.

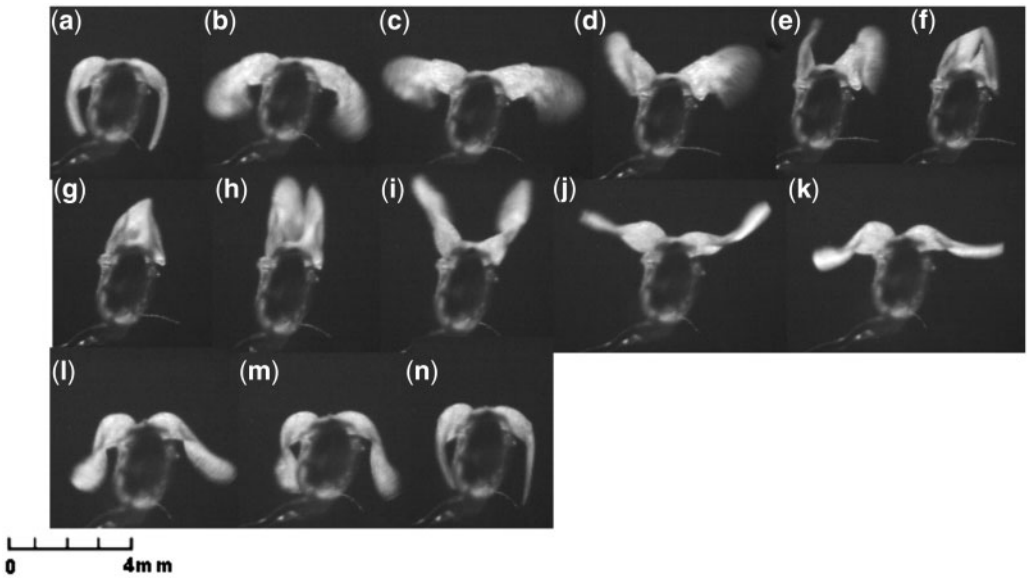


**Fig. 7** Posterior view of the stroke cycle of a large, tethered *L. helicina* starting from the recovery stroke. There are 16 ms between each frame shown.

and 10f). The wings then are flung out at the start of the power stroke, corresponding to the ''fling'' phase (Figs. 6g–h, 7h–I, 9g and 10g). Figure 11 illustrates this phenomenon for the large individual. The wings come together along the margin of the distal wing chord for about 12–16 ms and then detach along this same margin, taking about 16 ms to complete. The clap-and-fling appears to take about 28 ms or about 15% of the stroke cycle for a large *L. helicina*. Note also an additional interaction of the wings and the shelled body shown in Fig. 9B. In this sequence, the wings clap against the shell before entering the recovery stroke. The wings touch at the end of the downstroke and remain attached to either side of the shelled body of the medium pteropod for 8 ms and then begin peeling off the sides until detached after 8 ms.

A posterior view of the large tethered pteropod revealed left–right asymmetry. The wings of the large tethered animal move through more than one plane so measurements derived from two-dimensional data should be considered with caution. The distal edge of the left wing demonstrates a rather symmetrical angular displacement up to 125° before reaching a peak at 135° in posterior view (Fig. 12A). The angular displacement of the right distal wing is both narrower in shape than that of the left wing and larger, up to 177°. Indeed, there is a marked asymmetry between the amplitudes of the left and right wings between the interval of 48 and 128 ms ($P<0.001$). Left and right medial wing markers demonstrate comparable movements at the end of the power stroke; angles increase from a minimum, reflecting the untwisting of the wings from their

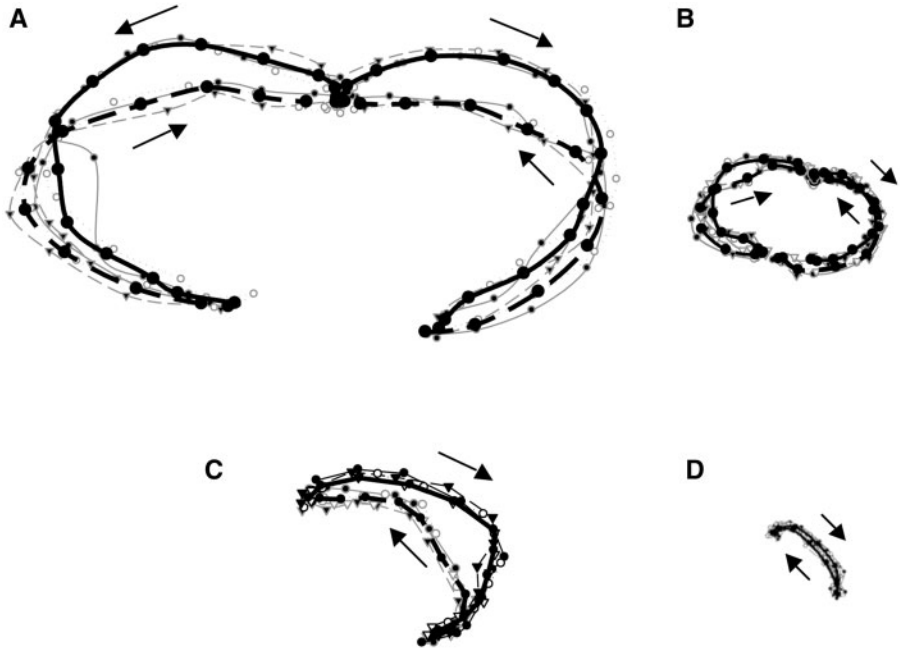


**Fig. 8** Two-dimensional wingtip paths for the three tethered *L. helicina* in this study. The posterior view of the large animal (A), dorsal view of the medium-sized animal (B), lateral views of the large (C) and small (D) individuals are shown with the dark lines representing the averaged paths. The wing course for the small individual has been rotated 45° from the tethered orientation to simplify comparison. The dark solid lines represent the mean power stroke of 5–10 paths while the dark dashed lines are the mean recovery strokes of 5–10 paths. Arrows show the direction of wing motion. The time between successive points is 8 ms.

perpendicular attitude to the dorsoventral axis of the body. Velocity profiles of the left and right wingtips and medial wing chords are rather symmetric and have a similar pattern. The wings increase in speed during the recovery stroke, falling to $0^\circ\,ms^{-1}$ at the middle of the stroke and then continue to increase negatively during the power stroke (Fig. 12B). The right medial wing has a maximum value of 81.7° at the start of the power stroke while this is achieved for the left wing at the end of the recovery stroke at 70.7°. The medial wing angular position exhibits a gradual rise in the recovery stroke and then, a similar gradual decrease, interrupted by a change in slope representing the moment that the wing untwists halfway into the power stroke. The increased displacement of the left wing about 32 ms into the stroke clearly demonstrates the fast wing rotation in the lateral view of the large animal (Fig. 12C and D). This motion actually involves an asymmetry in geometry with the wing accelerating from the sagittal plane followed by a deceleration as it continues to complete the half stroke in the transverse plane.

Asymmetry in wing orientation is not present in the motion of either the medium-sized or small *L. helicina*. The medium-sized animal has analogous left and right wing kinematics until after the onset of the power stroke past the 88 ms mark (Fig. 13A; $P<0.0001$). Angular movements are symmetric for the right wing (tip) leading up to a maximum displacement of 175.2° for the wingtip. The left wing (tip) has a lesser maximum amplitude of 160.7° with the two half strokes correspondingly less. The twisting of the wing that occurs in the large animal in the power stroke also is found in the medium animal. This is demonstrated by the increase in angular displacement at the end of this stroke as the wing returns to a straight state. Angular velocities also are equivalent for power and recovery strokes for left and right wings and also are comparable to those of the medial wing chords (Fig. 13B). The left wing of the small pteropod has an angular distal displacement of the tip of up to 176.1° with a very symmetric contour (Fig. 14A); this is in contrast to that of the large animal in the same lateral view, which shows a large angular increase of 16 ms duration and a very irregular profile (Fig. 12D). The small individual also had a more steady increase in velocity and a subsequent decrease during the recovery stroke of the wingtip (Fig. 14B). The medial wing position exhibits small angular deviations (only up to 44.8°) with very slight changes in velocity.

## Discussion

Swimming in *L. helicina* is a complex achievement, one in which the pteropod must overcome the weight of its shell and an asymmetry in body

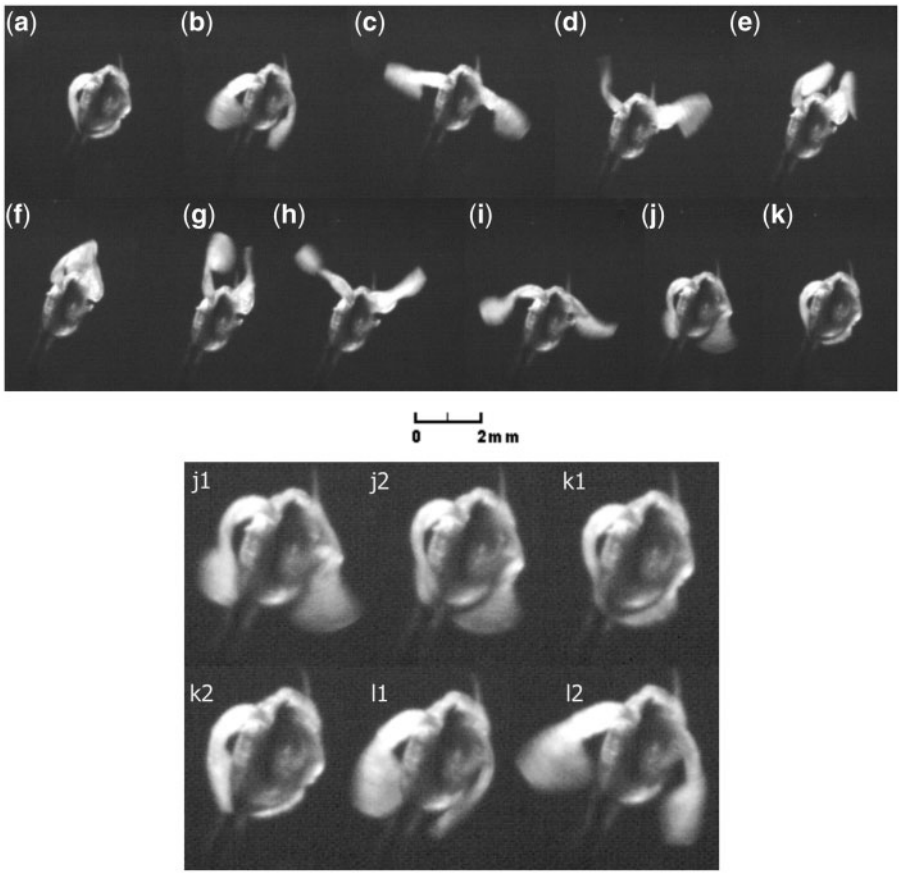


**Fig. 9** (A) Dorsal view of the stroke cycle of a medium-sized, tethered *L. helicina* starting from the recovery stroke. There are 16 ms between each frame shown. (B) Dorsal view of the stroke cycle of a medium, tethered *L. helicina*, starting from frame *j* with 8 ms between each frame. The power stroke ends with wingtips wrapping around the shelled body at *k*1. From *k*2 to *K*l2, the wings enter the recovery stroke, pulling away from the shelled body [See movies in Suppl. Data].

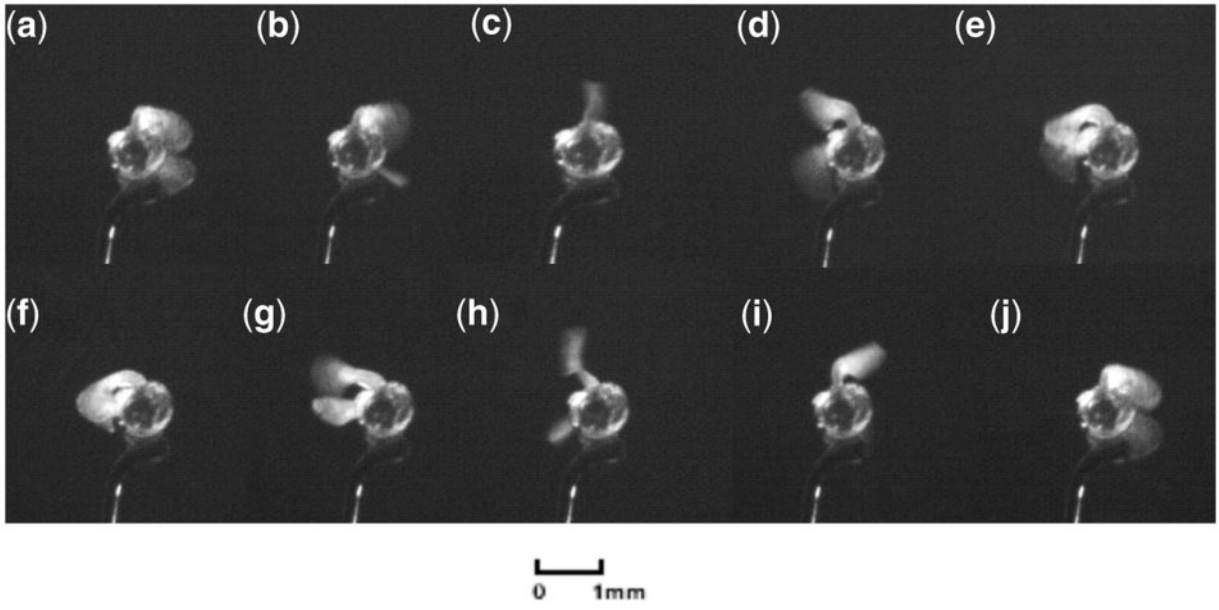


**Fig. 10** Lateral view of the stroke cycle of a small, tethered *L. helicina* starting from the recovery stroke. Note that the animal was tethered 45° from the normal, upright position. There are 12 ms between each frame shown.

**Table 2** Stroke periods for the three tethered *L. helicina* used in this study

| Shell diameter (mm) | Recovery stroke**(s) | Power stroke** (s) | Total period (s) |
|---|---|---|---|
| 3.10 ± 0.06 | 0.082 ± 0.011 | 0.109 ± 0.020 | 0.168 ± 0.029 |
| 1.98 ± 0.05 | 0.091 ± 0.013 | 0.078 ± 0.007 | 0.170 ± 0.012 |
| 0.94 ± 0.03 | 0.048 ± 0.004 | 0.058 ± 0.004 | 0.107 ± 0.003*** |

Means and standard deviations are of three to eight cycles for 13 sequences for the three individuals.
**$P < 0.01$; Paired sample *t*-tests between power and recovery stroke periods.
***$P < 0.0001$; analysis of variance of the total period between the three animals.

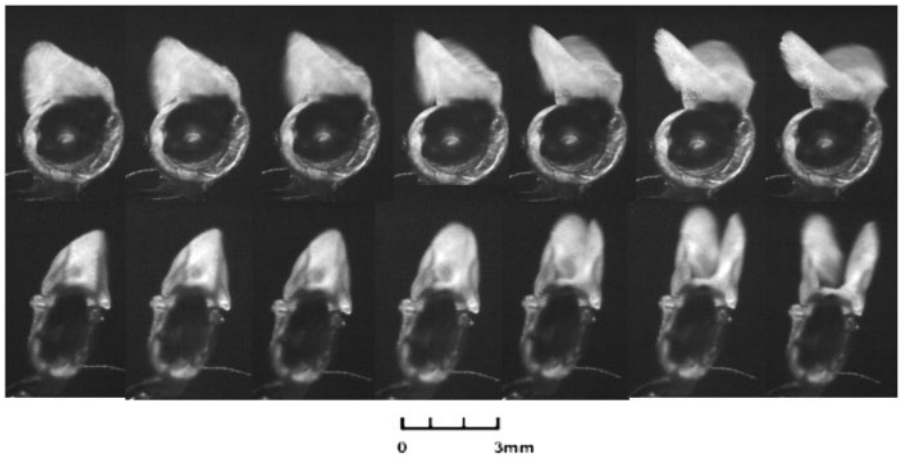


**Fig. 11** Clap-and-fling movements of parapodia of tethered *L. helicina* in lateral (top) and posterior (bottom) views; images are shown at 4 ms intervals.

structure to create upward movement. Underlying the many swimming forms utilized by *L. helicina* are the different objectives to be gained from underwater locomotion (Walker and Westneat 2000; Combes and Daniel 2001). For *L. helicina*, swimming serves functions such as evasion of predators, location of mates, and vertical migration. These activities require different locomotor attributes so it is not surprising that multiple swimming styles (helical versus linear ascents, flapping versus paddling, rotations and sinking) are used. Studies involving tethered organisms do not represent normal locomotor behaviors. Body pitching during *L. helicina* flapping is a good example of the kind of information that may be missed by not incorporating observations of unrestrained individuals. Changes in angle of the body are critical for the optimization of lift and the minimization of drag. Furthermore, the pattern of fluid circulation around the attached animal would have been disrupted (Dickinson 1996), resulting in an augmentation or even a diminution of swimming performance. Finally, restraining the animal prohibits an understanding of the full repertoire of behaviors. With that being said, tethering enables the capture and analysis of intricate high-speed motions of small animals.

## Size-dependent variation in the geometry and kinematics of the wing stroke

For planktonic organisms that exist in the intermediate Re range, inertial forces become increasingly important throughout development (Williams 1994). Reynolds numbers for the wing action ($Re_w$) varied between 35 and 380 with body size: the large individual has values of over 5× that of the medium and small *L. helicina* when corresponding views are compared (Table 3). Thus, the relative strengths of inertial to viscous forces experienced by the animals differ considerably with changes in size, reiterating the differences in stroke geometry that are found to increase at larger shell diameters. The larger pteropod is able to generate greater forward speed from the wing motion while the smaller advance ratio of the small animal suggests that flapping dominates and perhaps limits its movement. For most of *L. helicina* size range, sinking speeds exceeded swimming speeds except for the small pteropods, implying that the costs of upward movement increase substantially with body size and are a significant facet of the life cycle of mid and late stages.

The differences in the swimming kinematics observed in this study likely have to do with differences

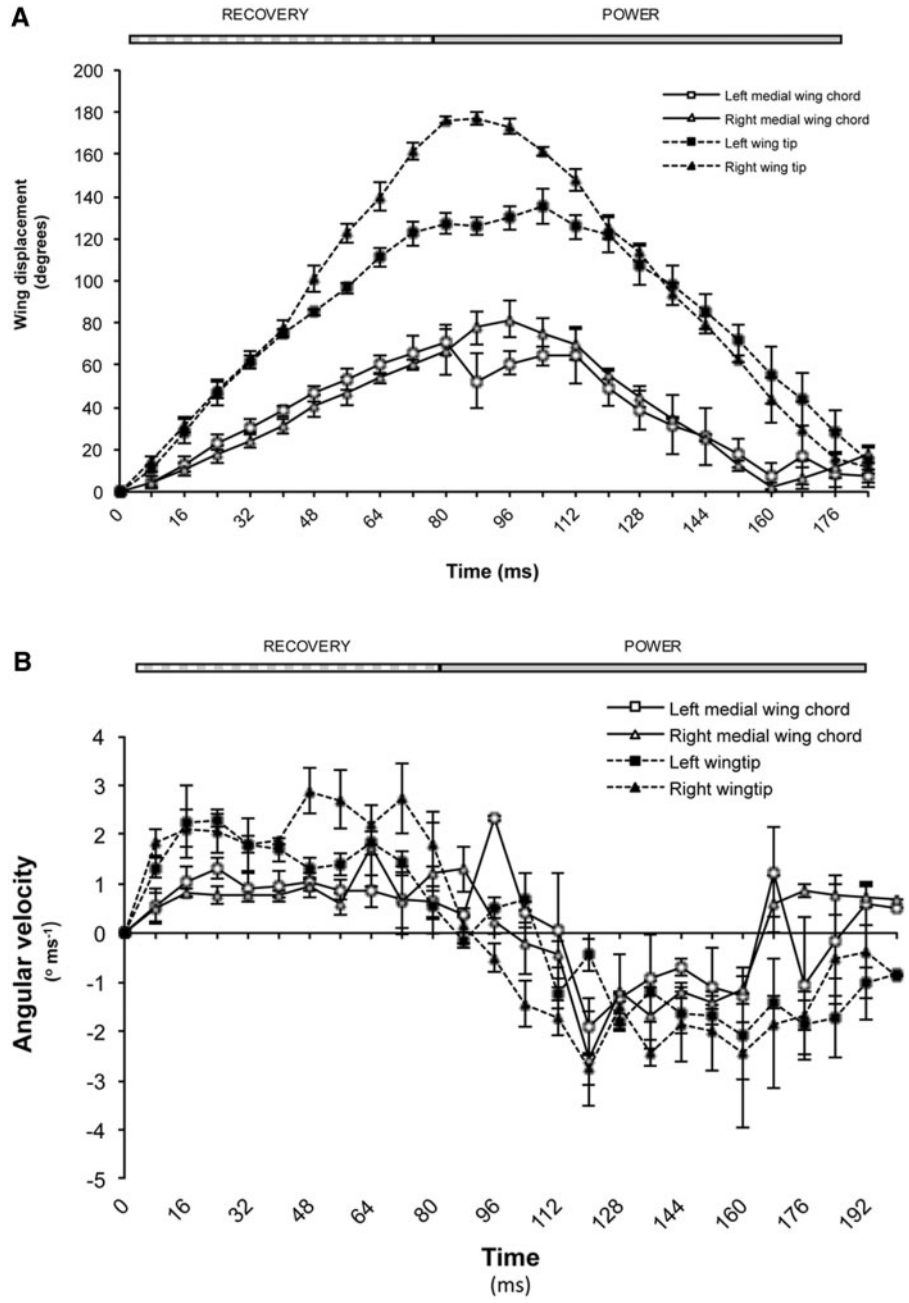


**Fig. 12** (A) Wing displacement of the large tethered *L. helicina* (posterior view). (B) Wing velocity of the large *L. helicina* (posterior view). (C) Wing displacement of the large *L. helicina* (lateral view). (D) Wing velocity of the large *L. helicina* (lateral view). For Figs. 12–14, means and standard deviations are taken from 4 to 7 strokes/wing with 13–25 positions/stroke. The power stroke is denoted in gray at the top of the figure.

in stroke geometry among the three tethered animals. The wing stroke of the small individual is characterized by the outer wing surface oscillating as a plate without any twisting. The flexible joint of the midchord acts like a hinge that moves little compared to the distal portions of the wing; a greater length of arc is moved in about the same amount of time as it takes the more proximal parts of the wing to traverse a smaller arc. The lack of wing flexion in the power stroke and the minimization of movement in the horizontal direction together maximize thrust in the vertical direction. The large individual exhibited substantial deviation of the wing stroke from the vertical axis and rotation of the wing at the initiation of the recovery stroke. The orientation of the appendages parallel to the direction of flow minimizes

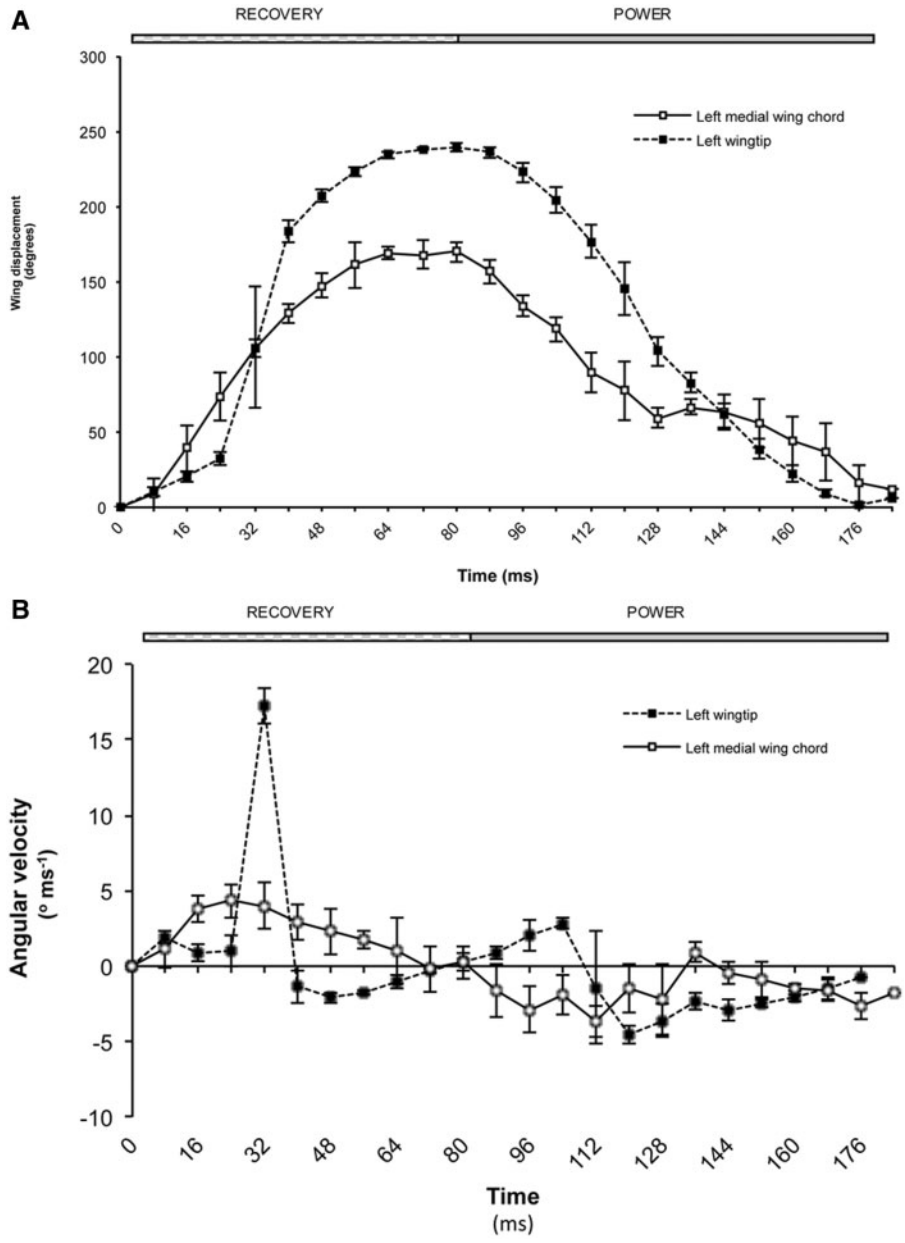


**Fig. 12** Continued.

the drag resistance to vertical swimming. In contrast, the small individual exhibited little rotation of the wing; the orientation of the wing may not matter at this low Re, as the change in drag coefficient is minimal when the orientation of the wing goes from perpendicular to parallel to the flow (Vogel 1994). During the midpoint of the power stroke, both large and small pteropods orient their wings in a high drag position perpendicular to the flow to generate thrust. However, the high flexibility of the large wings also may influence the degree of thrust available to the pteropod despite the orientation. The medium-sized animal displays an intermediate wing geometry that incorporates wing twisting in the power stroke but no wing rotation in the recovery stroke.

*Limacina helicina*'s kinematics are very different from those of the gymnosome pteropod *Clione antarctica* which lacks a calcareous shell. At 15°C, the swimming speed of *L. helicina* (1–3 mm) is 10–55 mm $s^{-1}$ or up to eight times faster (Re range = [20 380]) than that of *C. antarctica* (7–20 mm). *Clione antarctica* swims at 1–7 mm/s at −2°C (Re range = [6,123]; Borrell et al. 2005) and is neutrally buoyant (Seibel et al. 2007). In contrast, *L. helicina* sinks at a speed of 5–45 mm/s. For the 0.5 mg dry weight of the 3-mm pteropod, the

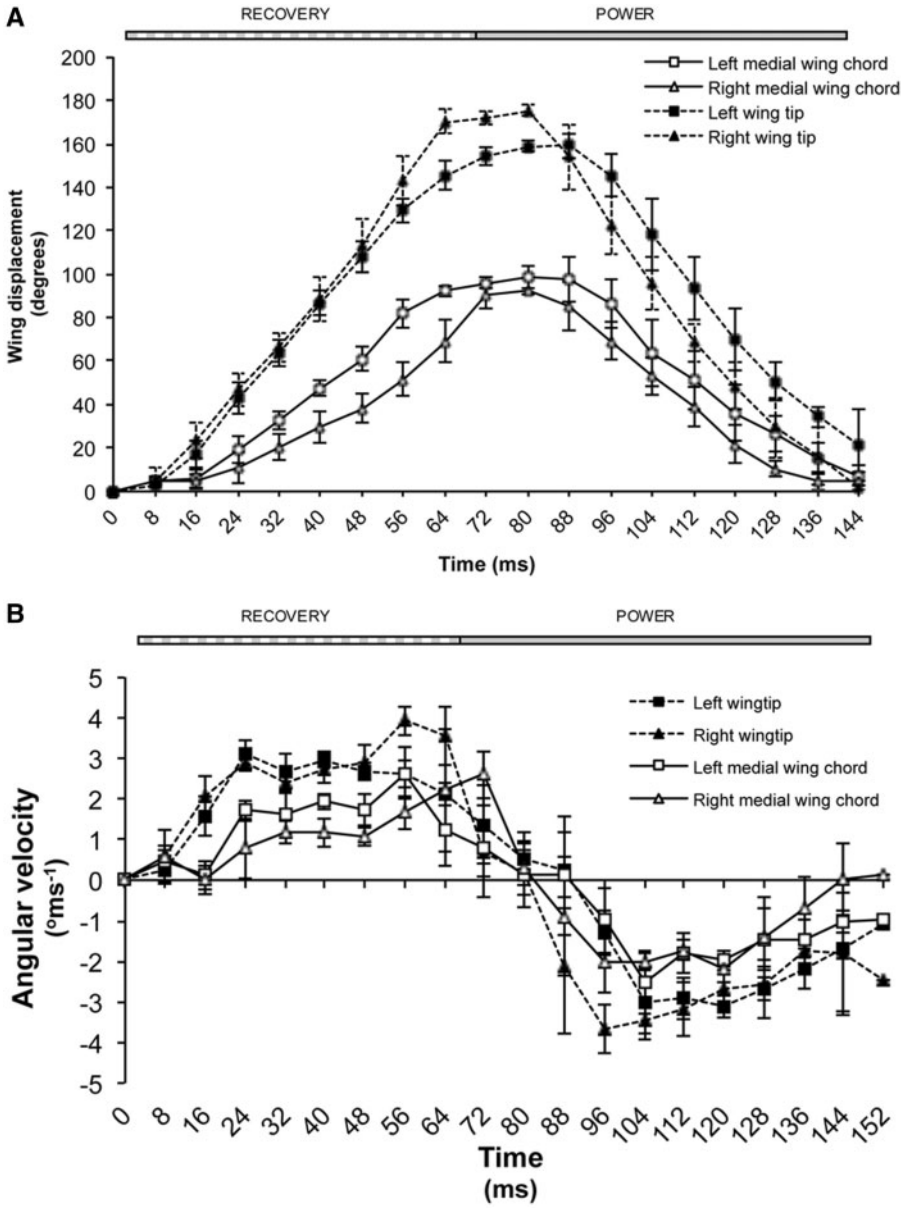


**Fig. 13** (A) Wing displacement of the medium-sized tethered *L. helicina* (dorsal view). (B) Wing velocity of the medium-sized *L. helicina* (dorsal view).

estimated terminal velocity of 40 mm/s corresponds well to the measured sinking speed. Sinking is a foremost force that governs the motion of this pteropod from intermediate to adult stages and most of the weight can be attributed to its aragonite shell. Given present concerns about thinning of shells due to effects of oceanic acidification on highly soluble aragonite (Seibel et al. 2007; Comeau et al. 2010; Hofman et al. 2010; Howard et al. 2011), reduced negative buoyancy may affect the balance of movements needed for efficient vertical travel and maneuvering ability. It is expected that oceanic acidification will result in undersaturation of calcium carbonate by 2016, becoming widespread by 2050, and that loss of these sentinels of anthropogenic increases in $CO_2$ may result in an ecological shift since thecosome pteropods are responsible for ingesting nearly half the primary production in the Southern Ocean and also serve as a primary food resource to upper trophic levels (Seibel and Fabry 2003; Orr et al. 2005).

### Rotational forces during swimming by *Limacina helicina*

*Limacina helicina* propels its way through water by beating its wings, thereby alternately rotating itself in opposing directions and generating continuous thrust. Torque forces are unmistakable in the swimming motion of *L. helicina*. The pteropod has an

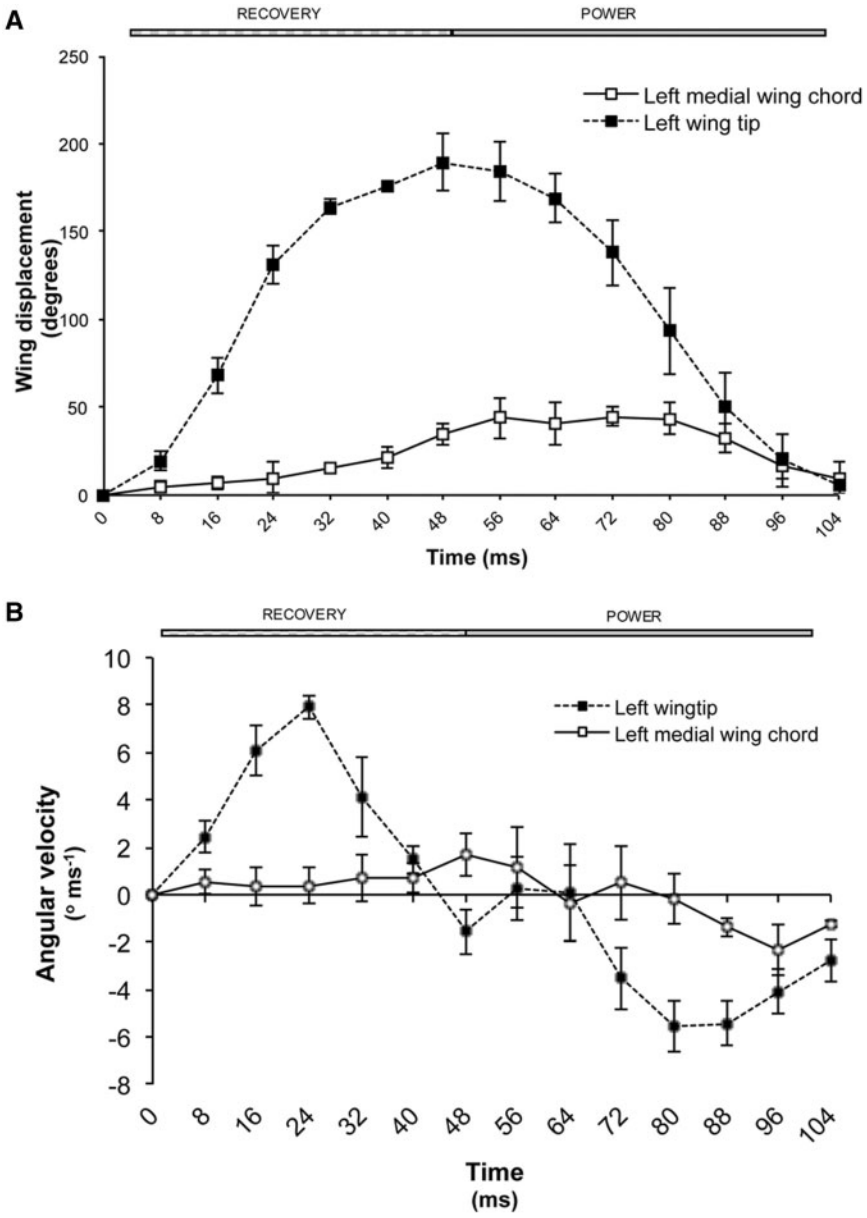


**Fig. 14** (A) Wing displacement of the small *L. helicina* (lateral view). (B) Wing velocity of the small *L. helicina* (lateral view).

**Table 3** Kinematic features of tethered *L. helicina* individuals and the subsequent Reynolds numbers and advance ratios

| View | Shell diameter (mm) | $Re_w$ | Stroke angle (o) | Advance ratio (J) |
|---|---|---|---|---|
| Posterior | 3.10 ± 0.06 | 380 ± 90 | 135.35 ± 8.42 | 0.74 |
| Dorsal | 1.98 ± 0.05 | 70 ± 13 | 160.74 ± 5.72 | 0.60 |
| Lateral | 0.94 ± 0.03 | 35 ± 6 | 189.22 ± 16.24 | 0.29 |
| Lateral | 3.10 ± 0.06 | 170 ± 45 | 239.53 ± 5.45 | 0.42 |

Means and standard deviations are of three to eight cycles for 13 sequences for the three individuals.
$Re_w$, J symbolize calculations performed on the left distal wingtip.

angular stroke plane where reciprocal rotation of the body occurs during the wing stroke, delineated by two half strokes. A pitching motion is caused by large stroke amplitudes (from 135° to 176°). The differences in stroke kinematics between left and right wings also contribute to a yawing motion, which is clearly evident in posterior views of the large tethered animal. The right distal wingtip has

a larger angle of stroke than does the left wing, an asymmetry that may reflect the fact that *L. helicina* is sinistrally-coiled. Although the shell's apex is not as large as in that of *L. retroversa*, the center of mass would be displaced somewhat to the left of the animal. The radial acceleration of the power stroke could result in the creation of lift on the wings while simultaneously rotating the animal in the opposite direction during the recovery stroke. Alternatively, if the center of mass is distant from the site of generation of force, a moment would be created, which also would rotate the pteropod (Nauen and Shadwick 2001). This disparity between the two sides has consequences for the pteropod, creating helical trajectories that may become more prominent as size increases. The medium-sized fixed animal has a wing stroke that is also suggestive of unevenness between the two sides, although to a lesser degree. This asymmetry makes the flapping motion unsteady and is implied by the advance ratios of less than 1. The erratic swimming of *L. helicina* recalls the flight of palatable butterflies that adopt highly erratic flight trajectories to avoid aerial predators (Kokshaysky 1977; Chai and Srygley 1990). *Limacina helicina* would similarly benefit from complex flight behavior to avoid predators such as *Clione limacina*.

Significant maneuverability while swimming upward during helical episodes demonstrates what also may be evasive behavior in the presence of potential predators. Maneuverability is enhanced both by the physical separation of wings by the shell and the use of propulsion by rowing. According to Dickinson (1996), greater directional control is gained when fluid interactions are uncoupled on either size of animal. The asymmetry in the left and right wing kinematics appears to compensate for the offset to the left of the center of mass toward the spiral of the shell. An example of their agility is their capacity for quickly sensing the approach of other individuals and steering to avoid collisions. It would be interesting, as a future study, to see if the inclusion of predators (*Clione*, fish) would change the swimming behavior of *L. helicina* from frequent straight ascents to perhaps a greater incidence of helical motion.

### Wing morphology and swimming performance

In air, optimal flight characteristics selects for long, narrow wings that are tapered, with high ARs and low wing loading (Combes and Daniel 2001). Seawater increases the magnitude of lift and drag by four times at an equivalent Re (Vogel 1994). This difference in density also increases the inertia of the wings by affecting not only the added mass but also the demand on the wing muscles. In an energetic perspective, short wings with high AR are thus favorable in seawater (Johansson and Aldrin 2002). In *L. helicina*, the distribution of the wing area is not equal when comparing medial wing chords since ARs decrease with increasing size. With greater area on the outer part of wing, more thrust can be generated but at the expense of efficiency for the large animal (Combes and Daniel 2001). Other contributors to the performance besides wing shape include unsteady effects (Daniel 1988) and wing flexion (Combes and Daniel 2001), two processes that are used by large individuals of *L. helicina*. Efficiency for the larger *L. helicina* may require that they generate more power to compensate for any deficit in energetics. Indeed, to exist in a fluid environment that is more inertial would require greater capacities for power. Another concern for *L. helicina* is the regulation of buoyancy. In addition to buoyancy control by bubbles and mucus feeding parachutes (Lalli and Gilmer 1989), it would appear that longer wings might benefit the animal by providing a greater surface area that would support more weight. In fact, *L. helicina* extends its wings as a means of arresting sinking and temporarily opposing the force of gravity.

All of the three *L. helicina* have ARs that are greater than five; the increased drag associated with low ARs ($AR < 5$) thus would be less of a concern (Combes and Daniel 2001). On the other hand, the high AR of the small pteropod suggests that it would be capable of effectively producing high levels of propulsion. In fact, the high frequency of wingbeat and great amplitude of stroke of the small individual enabled greater velocities to be achieved, indicating that the generation of force also would be considerable. This is in spite of the increased skin frictional drag on the skin associated with $Re < 100$ when viscous forces are prominent (Lehmann 2002). The stroke kinematics of smaller *L. helicina* may be more aerodynamically efficient than those of their larger counterparts. In a similar way, smaller fruit flies were able to generate greater total forces through slight changes in their stroke kinematics (Lehmann 2002). Greater coefficients of lift were possible through increases in mean angular velocity that were in turn accomplished by increasing the frequency of stroke for *Drosophila* sp. in a related study (Lehmann and Dickinson 1998).

The larger wing mass at the distal versus the proximal end also contributes to the rotation of the wings due to the large moment of inertia. Angular momentum depends on the product of the moment of

inertia and angular velocity. In turn, the moment of inertia is determined by the mass of the object as well as the distribution of this mass relative to the axis of rotation. Since the moment of inertia increases as the square of the distance of the mass, small increases in distance can have great effect on the angular momentum of an object. With greater chord length in the distal end, the larger animal has a larger moment of inertia and thus more angular momentum even when angular velocity is unchanged. Therefore, larger forces and more inertial power will be needed by the larger animals to carry out a wing stroke, hence, the inverse relationship with wingbeat frequency. This negative scaling of stride frequency is a common natural phenomenon and has been demonstrated for birds (Pennycuick 1996), insects (Lehmann and Dickinson 1998), fish (Drucker and Jensen 1996), as well as for a variety of other vertebrates (Heglund et al. 1974).

### Drag-based versus lift-based propulsion

*Limacina helicina* swims in the range of Re between 20 and 110 and flaps its parapodia in a range of Re of 35–380. The fluid regime that is experienced, thus, consists of both inertial and viscous components, conditions that are manifest in their mechanics of wing stroke. Both drag-based and lift-based mechanisms appear to be used in the wing kinematics of *L. helicina*. At midpoint in the power stroke, the wings are oriented horizontally or perpendicular to the direction of motion, creating propulsion in the vertical direction. The confinement of movement into one plane is easily seen in the kinematics of the small animal whose wing trajectory also traces a similar path. However, the wingtip paths reveal that the stroke's axis is posteroventral, which contradicts expectations of rowing mechanics when the paddle moves in the anteroposterior axis. With increases in body size, movements appear to be more complicated as flexion in the wings plays a larger role in the generation of force and there is more three-dimensionality to the wing stroke. Furthermore, pitching of the entire animal yields large stroke angles, which are uncharacteristic of normal rowing gaits as thrust is not confined to the vertical direction. It is possible that under these circumstances support for weight is created during the revolving power stroke and in the recovery stroke as the wings abduct to their clapped position.

The distinction between rowing and flapping is further obscured by the presence of an apparent lift-augmenting device that is present in the wing stroke of each of the tethered individuals. The phenomenon known as the clap-and-fling mechanism is a prominent feature in the flight of other small animals such as true butterflies, the wasp *Encarsia formosa*, *Drosophila* sp., and birds flying at slow speeds (Weis-Fogh 1973). Wings can contact each other to a variety of degrees, resulting in complete, partial, and near flings (Wakeling and Ellington 1997). Simulations using the immersed boundary method (Miller and Peskin 2009) show that when wings are flexible, as are the highly deformable wings of the pteropod, drag force is reduced and lift forces improved relative to those of a rigid wing. The pteropod does twist its wing at the halfway point of the downstroke, a mechanism noted to generate lift in fruit flies (Dickinson et al. 1999). In *L. helicina*, the presence of the shell makes complete contact of the two leading edges impossible. The ''wing'' tips of *L. helicina* touch at the end of the upstroke with direct clapping of the wing pair at the distal edges, while the wing bases are separated. For this reason, a partial fling would result. Other organisms with low Re show interesting differences in clap-and-fling behavior. In the tiny insects, the wings touch or nearly touch for most of the wingspan (Miller and Peskin 2009). The interference of the wings augments the circulation of water about each wing as they move rapidly downward, aided by the flow of fluid into the space created by separation of the wings (Weis-Fogh 1973). As a consequence, the amount of circulation *L. helicina* can generate increases, creating further weight support and thrust. Considering that movement is typically in the vertical direction, the clap and fling would be a crucial source of force production.

The shell is a solid body that could be used to create thrust through the acceleration of fluid between its surface and those of the wings. For the carridean shrimp, *Pandalus danae*, the technique of squeezing fluid between the tail and thorax results in a jet that propels the shrimp in a net backward direction (Daniel and Meyhofer 1989). It is possible that the power stroke of *L. helicina*, with the wing positioned so that the maximal surface area is pushing water against the shell, creates a jet that propels the animal during the recovery stroke. This additional source of propulsion may be needed to counter the weight of the calcareous shell.

## Conclusions

This study has provided some insight into the intricate motions involved in the swimming of a pelagic mollusc. Our analyses of the propulsion associated kinematics of the temperate pteropod,

*Limacina helicina*, show that pteropods locomote in an intermediate flow regime of Reynolds number ~10–100 where small changes in size, swimming speed, or viscosity can produce large changes in the fluid–organism interaction and pteropods have evolved a unique locomotory style that seems to take advantage of the balance between inertial and viscous forces. Like other animals, *L. helicina* displays an inverse relationship between wingbeat frequency and body size. In terms of its swimming mechanics, *L. helicina* has a distinctive swimming movement that propels the body in a radial axis, pitching negatively and positively during the stroke cycle. The power and recovery strokes executed by its flexible wing-like parapodia result in a sawtooth body trajectory that transports them during ascents and turns in the water column. Its erratic flight pattern is brought about by an asymmetry in the shell that manifests itself as an asymmetry between the angular displacements of the left and right wings. Size-based differences in stroke geometry also may reflect a greater capacity for power in larger animals and greater efficiency in smaller ones.

Swimming in *L. helicina* is unquestionably a distinct locomotion that cannot be evaluated in any simple manner. It remains difficult to characterize the wing motion of *L. helicina* as being strictly drag-based or lift-based as elements of both are incorporated. The wing is neither rigid and plate-like nor long and tapered at the distal end as needed to satisfy one or the other of these propulsion models. The pteropod wings exhibit flexibility and spanwise bending to a degree that is unmatched in any aerial flyers and the implications of this on force generation and propulsive efficiency are not understood. The axis of movement is radial and there seems to be a multitude of mechanisms that may be involved. Perhaps the most noteworthy observation of the present study is the use of a propulsion mechanism that is similar to the clap-and-fling mechanism noted in small flying invertebrates. While the frequency of wingbeat of this aquatic organism is 40 times slower than the 200-Hz wing flaps of insects (Dudley 2000), the Re is >10, considered to be the lower limit below which symmetric motion could not sustain a lift-based flapping mode of propulsion (Childress and Dudley 2004). The convergence of a mechanism into two disparate fluid media suggests that energetically, the clap-and-fling is a viable means of generating lift even in seawater, where drag forces are significantly greater than in air. Confirmation of the clap-and-fling mechanism awaits particle image velocimetric analyses of the circulation around the freely swimming pteropod, comparing those that flap perpendicular versus parallel to the direction of movement. With our new 3D tomography system (Murphy et al., submitted for publication), perhaps we will finally be able to see the circulation above the peeling wings and the downward jet as the wing collapses against the shell. Higher resolution flow fields are needed to assess whether the pteropods' flapping frequency is optimal for wake recapture to enhance lift (Wang 2000). Kinematic data as presented here plus empirical flow-field validation, using modern visualization techniques, are essential for the mathematical and computational fluid dynamic models that we are working on in an effort to examine the role of flexible appendages in the unusual propulsive mechanism of this small aquatic organism.

## Supplementary Data

Supplementary Data are available at *ICB* online.

## Acknowledgment

We thank Alice Alldredge for the opportunity to blue-water dive with her.

## Funding

The authors gratefully acknowledge financial support of the National Science Foundation (OCE 9907360/0296101 and CBET 0625898 to JY).

## References

Blake RW. 1981. Influence of pectoral fin shape on thrust and drag in labriform locomotion. J Zool 194:53–66.

Borrell BJ, Goldbogen JA, Dudley R. 2005. Aquatic wing flapping at low Reynolds numbers: swimming kinematics of the Antarctic pteropod, *Clione antarctica*. J Exp Biol 208:2939–49.

Chai P, Srygley RB. 1990. Predation and the flight, morphology, and temperature of neotropical rain-forest butterflies. Am Nat 135:748–65.

Childress S, Dudley R. 2004. Transition from ciliary to flapping mode in a swimming mollusc: flapping flight as a bifurcation in $Re_\omega$. J Fluid Mech 498:257–88.

Clark BD, Bemis W. 1979. Kinematics of swimming in penguins at the Detroit Zoo. J Zool 188:411–28.

Comeau S, Gorsky G, Alliouane S, Gattuso J-P. 2010. Larvae of the pteropod *Cavolinia inflexa* exposed to aragonite undersaturation are viable but shell-less. Mar Biol 157:2341–5.

Combes SA, Daniel TL. 2001. Shape, flapping and flexion: wing and fin design for forward flight. J Exp Biol 204:2073–85.

Daniel TL. 1988. Forward flapping flight from flexible fins. Can J Zool 66:630–8.

Daniel TL, Meyhofer E. 1989. Size limits in escape locomotion of carridean shrimp. J Exp Biol 143:245–65.

Dickinson MH. 1996. Unsteady mechanisms of force generation in aquatic and aerial locomotion. Am Zool 36:537–54.
Dickinson MH, Lehmann F-O, Sane SP. 1999. Wing rotation and the aerodynamic performance of model wings at low Reynolds numbers. J Exp Biol 174:45–64.
Drucker EG, Jensen JS. 1996. Pectoral fin locomotion in the striped surfperch. II. Scaling swimming kinematics and performance at a gait transition. J Exp Biol 199:2235–42.
Dudley R. 2000. The biomechanics of insect flight: form, function, evolution. Princeton: Princeton University Press.
Ellington CP. 1984. The aerodynamics of hovering insect flight. IV. Aerodynamic mechanisms. Philos Trans Roy Soc Lon B 305:79–113.
Fish FE. 1996. Transitions from drag-based to lift-based propulsion in mammalian swimming. Am Zool 36:628–41.
Gibb AC, Jayne BC, Lauder GV. 1994. Kinematics of pectoral fin locomotion in the bluegill sunfish *Lepomis macrochirus*. J Exp Biol 189:133–61.
Gilmer RW, Harbison GR. 1986. Morphology and field behavior of pteropod mollusks: feeding methods in the families Cavoliniidae, Limacinidae and Peraclididae (Gastropoda: Thecosomata). Mar Biol 91:47–57.
Heglund NC, Taylor CR, McMahon TA. 1974. Scaling stride frequency and gait to animal size: mice to horses. Science 186:1112–3.
Hofmann GE, Barry JP, Edmunds PJ, Gates RD, Hutchins DA, Klinger T, Sewell MA. 2010. The effect of ocean acidification on calcifying organisms in marine ecosystems: an organism to ecosystem perspective. Annu Rev Ecol Evol Syst 41:127–47.
Horridge GR. 1956. The flight of very small insects. Nature 178:1334–5.
Howard WR, Roberts D, Moy AD, Lindsay MCM, Hopcroft RR, Trull TW, Bray SG. 2011. Distribution, abundance and seasonal flux of pteropods in the sub-antarctic zone. Deep Sea Res II 58:2293–300.
Johansson LC, Aldrin BSW. 2002. Kinematics of diving Atlantic puffins (*Fratercula arctica* L.): evidence for an active upstroke. J Exp Biol 205:371–8.
Kokshaysky NV. 1997. Some scale dependent problems in aerial animal locomotion In: Pedley TJ, editor. Scale effects in animal locomotion. London: Academic Press. p. 421–35.
Lalli CM, Gilmer RW. 1989. Pelagic snails: the biology of Holoplanktonic gastropod mollusks. Stanford, CA: Stanford University Press.
Lehmann F-O. 2002. The constraints of body size on aerodynamics and energetics in flying fruit flies: an integrative view. Zoology 105:1–9.
Lehmann F-O, Dickinson MH. 1998. The control of wing kinematics and flight forces in fruit flies (Drosophila spp.). J Exp Biol 201:385–401.
Miller MA, Peskin CS. 2004. When vortices stick: an aerodynamic transition in tiny insect flight. J Exp Biol 207:3073–88.
Miller MA, Peskin CS. 2009. Flexible clap and fling in tiny insect flight. J Exp Biol 212:3076–90.
Morton JE. 1958. The Biology of *Limacina retroversa*. J Marine Biol Assoc 33:297–312.
Nauen JC, Shadwick RE. 2001. The dynamics and scaling of force production during the tail-flip escape response of the California spiny lobster *Panulirus interruptus*. J Exp Biol 204:1817–30.
Orr JC, Fabry VJ, Aumont D, Bopp L, Doney SC, Feely RA, Gnanadesikan A, Gruber N, Ishinda A, Jacobs F, et al. 2005. Anthropogenic ocean acidification over the twenty-first century and its impacts on calcifying organisms. Nature 437:481–6.
Pennycuick C. 1996. Wingbeat frequency of birds in steady cruising flight: new data and improved predictions. J Exp Biol 199:1613–8.
Renous S, Bels V. 1993. Comparison between aquatic and terrestrial locomotions of the leatherback sea turtle (*Dermochelys coriacea*). J Zool 230:357–78.
Rosenberger LJ, Westneat MW. 1999. Functional morphology of undulatory pectoral fin locomotion in the stingray Taeniura lymma (Chondrichthyes: Dasyatidae). J Exp Biol 202:3523–39.
Satterlie RA, LaBarbera M, Spencer AN. 1985. Swimming in the pteropod mollusk, *Clione limacina*. J Exp Biol 59:189–204.
Seibel BA, Fabry VJ. 2003. Marine biotic response to elevated carbon dioxide. Adv Appl Biodiver Sci 4:59–67.
Seibel BA, Dymowska A, Rosenthal J. 2007. Metabolic temperature compensation and coevolution of locomotory performance in pteropod molluscs. Integr Comp Biol 47:880–91.
Spedding GR, Maxworthy T. 1986. The generation of circulation and lift in a rigid two-dimensional fling. J Fluid Mech 165:247–72.
Stokes MD. 1997. Larval locomotion of the lancelet *Branchiostoma floridae*. J Exp Biol 200:1661–80.
Szymik BG, Satterlie RA. 2011. Changes in wingstroke kinematics associated with a change in swimming speed in a pteropod mollusk, *Clione limacina*. J Exp Biol 214:3935–47.
Vogel S. 1994. Life in moving fluids. Princeton: Princeton University Press.
Wakeling JM, Ellington CP. 1997. Dragonfly flight II. Velocities, accelerations and kinematics of flapping flight. J Exp Biol 200:557–82.
Walker JA. 2002. Functional morphology and virtual models: physical constraints on the design of oscillating wings, fins, legs, at intermediate Reynolds numbers. Integr Comp Biol 42:232–42.
Walker JA, Westneat MW. 2000. Mechanical performance of aquatic rowing and flying. Proc Roy Soc Lon B 267:1875–81.
Wang ZJ. 2000. Two dimensional mechanism for insect hovering. Phys Rev Lett 85:2216–8.
Webb PW. 1973. Kinematics of pectoral fin propulsion in *Cymatogaster aggregate*. J Exp Biol 59:697–710.
Weis-Fogh T. 1973. Quick estimates of flight fitness in hovering animals, including novel mechanisms for lift production. J Exp Biol 59:169–230.
Williams TA. 1994. A model of rowing propulsion and the ontogeny of locomotion in *Artemia* larvae. Bio Bull 187:164–73.
Wormuth JH. 1981. Vertical distributions and diel migrations of Euthecosomata in the northwest Sargasso Sea. Deep-Sea Res 28 A:1493–515.